PROCEEDINGS OF THE ROYAL SOCIETY A

Proc. R. Soc. A (2007) **463**, 961–977
doi:10.1098/rspa.2006.1802
Published online 9 January 2007

The *N*-vortex problem on a rotating sphere. III. Ring configurations coupled to a background field

By Paul K. Newton[1,*] and Takashi Sakajo[2]

[1]*Department of Aerospace & Mechanical Engineering and Department of Mathematics, University of Southern California, Los Angeles, CA 90089-1191, USA*
[2]*Department of Mathematics, Hokkaido University, Sapporo 060-0810, Japan*

We study the evolution of *N*-point vortices in ring formation embedded in a background flowfield that initially corresponds to solid-body rotation on a sphere. The evolution of the point vortices is tracked numerically as an *embedded* dynamical system along with the *M* contours which separate strips of constant vorticity. The full system is a discretization of the Euler equations for incompressible flow on a rotating spherical shell, hence a 'barotropic' model of the one-layer atmosphere. We describe how the coupling creates a mechanism by which energy is exchanged between the ring and the background, which ultimately serves to break up the structure. When the centre-of-vorticity vector associated with the ring is initially misaligned with the axis of rotation of the background field, it sets up the propagation of Rossby waves around the sphere which move retrograde to the solid-body rotation. These waves pass energy to the ring (in the case when the solid-body field and the ring initially co-rotate) or extract energy from the ring (when the solid-body field and the ring initially counter-rotate), hence the Hamiltonian and the centre-of-vorticity vector associated with the *N*-point vortices are no longer conserved as they are for the one-way coupled model described by Newton & Shokraneh. In the first case, energy is transferred to the ring, the length of the centre-of-vorticity vector increases, while its tip spirals in a clockwise manner towards the North Pole. The ring stays relatively intact for short times, but ultimately breaks-up on a longer time-scale. In the latter case, energy is extracted from the ring, the length of the centre-of-vorticity vector decreases while its tip spirals towards the North Pole and the ring loses its coherence more quickly than in the co-rotating case. The special case where the ring is initially oriented so that its centre-of-vorticity vector is perpendicular to the axis of rotation is also examined as it shows how the coupling to the background field breaks this symmetry. In this case, both the length of the centre-of-vorticity vector and the Hamiltonian energy of the ring achieve a local maximum at roughly the same time.

Keywords: *N*-vortex problem; rotating sphere; background vorticity gradients; embedded dynamical system

* Author for correspondence (newton@usc.edu).

Received 15 August 2006
Accepted 28 November 2006

1. Introduction

We study the evolution of a ring of N-point vortices on a sphere embedded in a background flow that initially corresponds to solid-body rotation. Our main goal is to understand the nature of the coupling between the ring and the background field in order to elucidate the mechanism by which such configurations, which model the boundary between distributed coherent vortices and the backgrounds in which they are embedded, are destabilized in much more complex settings. The paper by McDonald (1999) provides an excellent discussion of many of the key effects associated with geophysical vortices. We adopt a simple barotropic vorticity model on the sphere (as in DiBattista & Polvani 1998) in order to identify several key features of the interaction process in a pristine environment, where definitive statements can be made based on careful numerical experiments and comparisons with the simpler one-way coupled model developed in Parts I, II and IV of this sequence (see Jamaloodeen & Newton 2006; Newton & Shokraneh 2006*a*,*b*). In particular, Part I in this sequence highlighted the importance of the misalignment of the centre-of-vorticity vector associated with the N-point vortices with the axis of rotation associated with the solid-body velocity field. In this paper, we include the additional important physical mechanism of coupling to the background flow and the subsequent generation of Rossby waves; hence, we are able to understand the combined effects of the misalignment and coupling when both act together. The strength of this approach is in our ability to isolate the key mechanisms which lead to the ring breakup and loss of integrable structure of the one-way coupled model that was established in Part I. Of course, when analysing more complex systems such as Jupiter's atmosphere (Marcus 1993), the distinction between the vorticity associated with a coherent structure, such as the Great Red Spot, and the background vorticity is far less clear.

(*a*) *Summary of the one-way coupled model*

We first summarize the one-way coupled model in order to contrast its main features with the two-way coupled model studied in this paper. In Part I of this sequence (see Newton & Shokraneh 2006*a*), we introduced a model for the evolution of N-point vortices on a sphere with background solid-body rotational velocity field. The dynamical system for the N-point vortices is given by

$$\dot{\boldsymbol{x}}_\alpha = \frac{1}{4\pi}\sum_{\beta=1}^{N}{}' \Gamma_\beta \frac{\boldsymbol{x}_\beta \times \boldsymbol{x}_\alpha}{(1-\boldsymbol{x}_\alpha\cdot\boldsymbol{x}_\beta)} + \Omega\hat{\boldsymbol{e}}_z \times \boldsymbol{x}_\alpha \quad (\alpha = 1,\ldots,N) \quad \boldsymbol{x}_\alpha \in \mathbb{R}^3, \quad \|\boldsymbol{x}_\alpha\| = 1. \tag{1.1}$$

The prime on the summation indicates that the singular term $\beta = \alpha$ is omitted and, initially, the vortices are located at the given positions $\boldsymbol{x}_\alpha(0) \in \mathbb{R}^3$, $(\alpha = 1, \ldots, N)$. The denominator in (1.1) is the chord distance between vortex Γ_α and Γ_β since $\|\boldsymbol{x}_\alpha - \boldsymbol{x}_\beta\|^2 = 2\,(1-\boldsymbol{x}_\alpha\cdot\boldsymbol{x}_\beta)$. The first term on the right-hand side is the discrete Biot–Savart law (see Newton 2001), while the last term represents a solid-body rotational velocity field, with axis of rotation aligned with the North–South polar axis (i.e. the z-axis). As emphasized in Part I, the solid-body rotation affects the dynamics of the N-point vortices, but the vortices do not alter the 'background' flow, which remains in solid-body form. Hence, we called this a one-way coupled model.

The key to understanding this simplified model is the realization that the *centre-of-vorticity* vector $\boldsymbol{J}$ associated with the point vortices, defined as

$$\boldsymbol{J} = \sum_{\alpha=1}^{N} \Gamma_\alpha \boldsymbol{x}_\alpha = \left(\sum_{\alpha=1}^{N} \Gamma_\alpha x_\alpha, \sum_{\alpha=1}^{N} \Gamma_\alpha y_\alpha, \sum_{\alpha=1}^{N} \Gamma_\alpha z_\alpha \right) = (J_x, J_y, J_z), \tag{1.2}$$

satisfies

$$\dot{\boldsymbol{J}} = \Omega \hat{\boldsymbol{e}}_z \times \boldsymbol{J}, \tag{1.3}$$

as can be verified by multiplying (1.1) by Γ_α, summing over α and using the fact that $\boldsymbol{x}_\alpha \times \boldsymbol{x}_\beta = -\boldsymbol{x}_\beta \times \boldsymbol{x}_\alpha$. Equation (1.3) is solved by applying the rotation matrix, $\boldsymbol{M}_\Omega(t)$, to $\boldsymbol{J}(0)$,

$$\boldsymbol{J}(t) = \boldsymbol{M}_\Omega(t) \boldsymbol{J}(0). \tag{1.4}$$

$\boldsymbol{M}_\Omega(t)$ is given by

$$\boldsymbol{M}_\Omega(t) = \begin{pmatrix} \cos \Omega t & -\sin \Omega t & 0 \\ \sin \Omega t & \cos \Omega t & 0 \\ 0 & 0 & 1 \end{pmatrix}, \tag{1.5}$$

and is a unitary matrix with the property

$$\boldsymbol{M}_\Omega^{\mathrm{T}} = \boldsymbol{M}_\Omega^{-1}; \qquad \boldsymbol{M}_\Omega(0) = \boldsymbol{I}. \tag{1.6}$$

From this, we conclude that the length of $\boldsymbol{J}$ is constant since

$$\begin{aligned} \|\boldsymbol{J}\|^2 = \langle \boldsymbol{J}, \boldsymbol{J} \rangle = \langle \boldsymbol{M}_\Omega \boldsymbol{J}(0), \qquad \boldsymbol{M}_\Omega \boldsymbol{J}(0) \rangle = \langle \boldsymbol{M}_\Omega^{\mathrm{T}} \boldsymbol{M}_\Omega \boldsymbol{J}(0), \\ \boldsymbol{J}(0) \rangle = \|\boldsymbol{J}(0)\|^2, \end{aligned} \tag{1.7}$$

while the components break up into two conserved quantities,

$$J_x^2 + J_y^2 = C_1 = \text{const.} \tag{1.8}$$

$$J_z = C_2 = \text{const.} \tag{1.9}$$

The remaining important conserved quantity is the Hamiltonian, H, given by

$$H = -\frac{1}{4\pi} \sum_{\alpha<\beta}^{N} \Gamma_\alpha \Gamma_\beta \log \|\boldsymbol{x}_\alpha - \boldsymbol{x}_\beta\|. \tag{1.10}$$

As the N-vortices evolve under their mutual interaction around $\boldsymbol{J}$, it in turn rotates with frequency Ω about the z-axis, maintaining a fixed angle γ with respect to the axis. See Part I for more details.

We made the simple observation that it is the *misalignment* of the centre-of-vorticity vector with the axis of rotation ($\gamma \neq 0$) that is an important ingredient in understanding the dynamics of the vortices. The key to understanding the ramifications of the misalignment is to understand how the unitary operator, $\mathcal{L}_\Omega^{\boldsymbol{J}}(t)$, affects trajectories on the aligned ($\gamma = 0$) non-rotating ($\Omega = 0$) sphere. The relation between solutions of the original rotating system,

$\boldsymbol{x}_\alpha(t)$, and solutions of the aligned non-rotating system, $\boldsymbol{z}_\alpha(t)$, is via the linear operator $\mathcal{L}^{\boldsymbol{J}}_{\Omega}(t) \equiv \boldsymbol{M}_{\Omega}(t)\boldsymbol{M}_z^{-1}\boldsymbol{M}_y^{-1}$

$$\boldsymbol{x}_\alpha(t) = \mathcal{L}^{\boldsymbol{J}}_{\Omega}(t)\boldsymbol{z}_\alpha(t). \tag{1.11}$$

The matrices $\boldsymbol{M}_y$ and $\boldsymbol{M}_z$ serve to align $\boldsymbol{J}(0)$ with the z-axis, hence are defined as

$$\boldsymbol{M}_z = \begin{pmatrix} \cos\gamma_z & -\sin\gamma_z & 0 \\ \sin\gamma_z & \cos\gamma_z & 0 \\ 0 & 0 & 1 \end{pmatrix}, \tag{1.12}$$

$$\boldsymbol{M}_y = \begin{pmatrix} \cos\gamma_y & 0 & \sin\gamma_y \\ 0 & 1 & 0 \\ -\sin\gamma_y & 0 & \cos\gamma_y \end{pmatrix}. \tag{1.13}$$

We note that the operator $\mathcal{L}^{\boldsymbol{J}}_{\Omega}(t)$ is time dependent, but more importantly contains information on the original alignment of $\boldsymbol{J}$ with the axis of rotation. It was emphasized that understanding the effects of this operator on time-dependent trajectories was the key towards understanding the effects of rotation. The shortcomings of this model are that the background rotational velocity field is not altered by the presence of the N-point vortices, so there is no exchange of energy between the N-vortex field and the background flow. As a result, the system cannot support the propagation of Rossby waves which are known to be an essential ingredient in many dynamical atmospheric processes (Hoskins 1973; Pedlosky 1987; Majda 2003). In addition, the stability characteristics (see Cabral *et al.* 2003) and integrability (Bogomolov 1977, 1979, 1985; Kidambi & Newton 1998, 2000; Newton & Shokraneh 2006*a*) of the pure N-vortex problem on the non-rotating sphere remains largely intact in this one-way coupled model.

The goal of the current paper is to understand the effects of coupling the background field to the point-vortex dynamics, with particular attention paid to the misalignment of the $\boldsymbol{J}$ vector. We will elucidate the effect of the two-way coupling to the dynamics of the N-point vortices, which are embedded in the background field and are able to exchange energy with it. The model we adopt, called a one-layer spherical barotropic model, was used in DiBattista & Polvani (1998) to understand the evolution of dipoles. What was not emphasized in that study is the role the misalignment plays in the overall dynamical processes. In fact, if the centre-of-vorticity vector is initially aligned with the axis of rotation, then this effect plays no role. To set the stage for the descriptions to follow, we show in figure 1 the schematic diagram associated with the point-vortex ring and the discretized background field described in more detail later. Note the initial misalignment of $\boldsymbol{J}$ with the axis of rotation as characterized by setting $\gamma \neq 0$ initially. As the ring and the background strips evolve (as shown in figure 2), the $M-1$ contours associated with the M strips deform and wrap around the point vortices, while the ring is destabilized and ultimately destroyed. Details of this process, with particular emphasis on the exchange of energy between the ring and the background, follow in §§3 and 4 after a description of the numerical method.

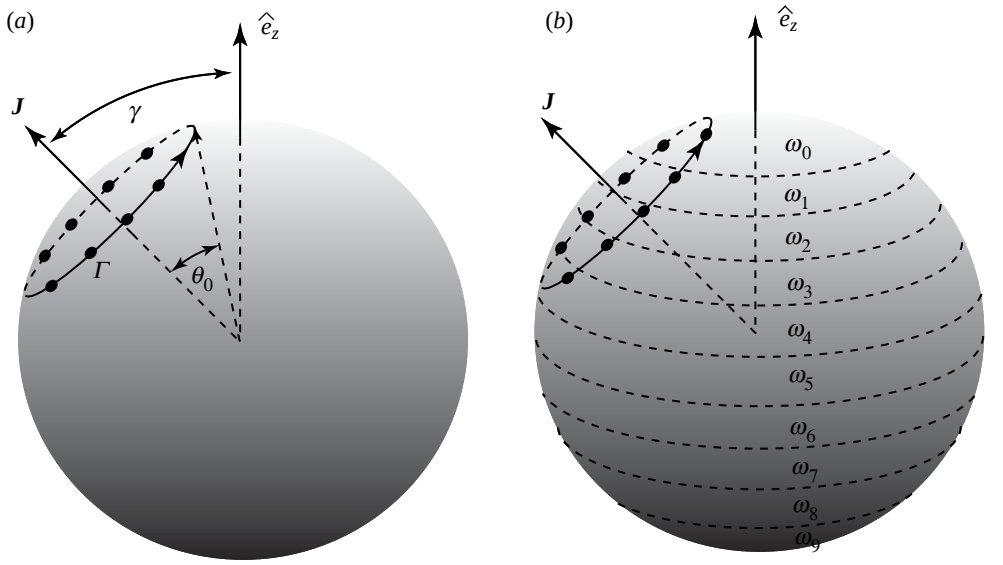

Figure 1. Initial configuration with N equal strength point vortices (Γ) evenly spaced around a spherical cap which gives rise to the $\boldsymbol{J}$ vector as shown. (a) The size of the spherical cap is characterized by the base half-angle θ_0, while the orientation with respect to the axis of rotation is characterized by angle γ. (b) Ten constant vorticity strips ω_n=constant with nine contours that require tracking. The constant values ω_n are chosen so that they approximate the vorticity distribution corresponding to solid-body rotation around the z-axis. See text for more details.

2. The numerical method

The numerical method we use is based on that described by DiBattista & Polvani (1998). The vorticity on the unit sphere evolves according to the equation $\mathrm{D}\omega/\mathrm{D}t=0$, where $\omega=\boldsymbol{x}\cdot(\nabla\times\boldsymbol{u})$ and $\boldsymbol{u}$ is the two-dimensional velocity field. The incompressibility condition $\nabla\cdot\boldsymbol{u}=0$ implies the existence of streamfunction $\psi(\boldsymbol{x})$, where $\boldsymbol{u}=\boldsymbol{x}\times\nabla\psi$, which gives rise to the relation $\omega=\Delta\psi$. Inversion of this expression gives rise to

$$\psi(\boldsymbol{x}) = \int\int_S G(\boldsymbol{x},\boldsymbol{x}')\omega(\boldsymbol{x})\mathrm{d}A, \tag{2.1}$$

where $G(\boldsymbol{x},\boldsymbol{x}')$ is the Green's function on the sphere $G(\boldsymbol{x},\boldsymbol{x}')=-(1/4\pi)\log|\boldsymbol{x}-\boldsymbol{x}'|^2$. As in Bogomolov (1977, 1979), we think of the vorticity field as being made up of two parts, $\omega(\theta,\phi)=\omega_N+\omega_{SB}$. ω_N is the vorticity due to the N-point vortices, i.e.

$$\omega_N = \frac{1}{\sin\theta}\sum_{\alpha=1}^{N}\Gamma_\alpha\delta(\theta-\theta_\alpha,\phi-\phi_\alpha), \tag{2.2}$$

where $(\theta_\alpha,\phi_\alpha)$ represents the position of the αth point vortex in spherical coordinates. This gives rise to the velocity field

$$\boldsymbol{u}_{\boldsymbol{v}}(\boldsymbol{x}) = \frac{\Gamma}{4\pi}\sum_{\alpha=1}^{N}\frac{\boldsymbol{x}_\alpha\times\boldsymbol{x}}{1-\boldsymbol{x}\cdot\boldsymbol{x}_\alpha}. \tag{2.3}$$

The initial configuration of the misaligned N-vortex ring as in figure 1a is given as follows. First, the N-vortex points are equally spaced along a line of latitude

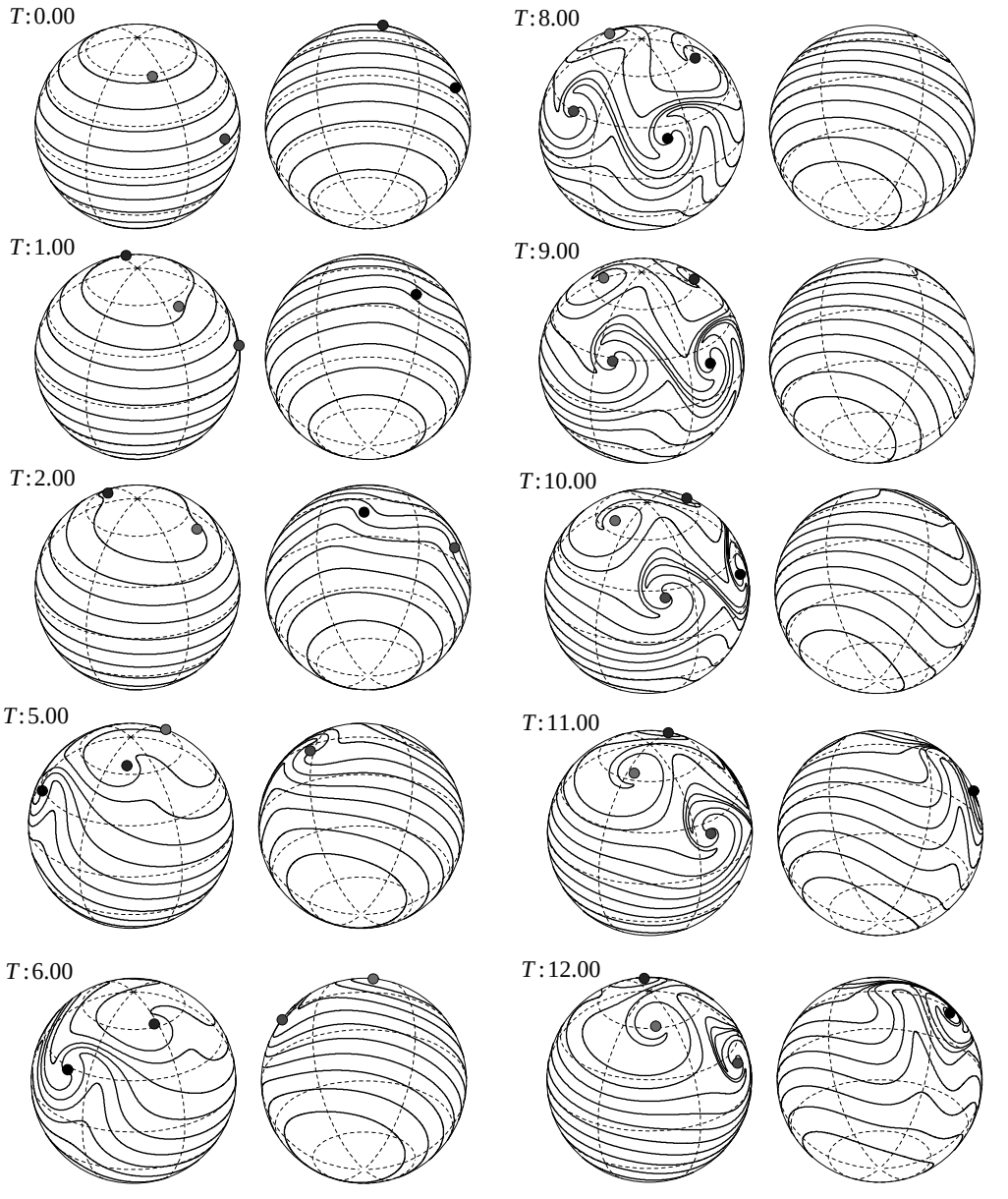

Figure 2. Evolution of ring configuration and contours with $N=4$ and $M=10$ and frequency ratio $4:1$. Orientation $\gamma=\pi/4$ and $\theta_0=\pi/4$. $T=0.00$–12.00 in dimensionless units. Note that the wrapping of the contours around the point vortices effectively increases their strength with respect to the background. The ring stays relatively intact throughout the evolution.

$z=\cos\theta_0$, then they are rotated around the x-axis by the angle γ. The strength of each vortex point Γ is determined so that the frequency ratio between the ring's rotation frequency and the solid-body frequency becomes $m:n$, namely

$$\omega : \Omega = \frac{\Gamma(N-1)\cos\theta_0}{4\pi\sin^2\theta_0} : \frac{1}{2} = m : n. \tag{2.4}$$

The second part of the vorticity field, ω_{SB}, is thought of as the 'background' vorticity, which for our model initially corresponds to the solid-body rotation. This is discretized by $M+1$ zonal strips of uniform vorticity separated by latitudinal contours, which we track numerically (see figure 1*b*). Let $\boldsymbol{X}_\alpha(\theta, t)$ $\alpha=1, \ldots, M$ represent the M contour curves, in which $0\leq\theta<2\pi$ is a parameter along the contour curve and t is time. The initial position of $\boldsymbol{X}_\alpha$ is given by

$$\boldsymbol{X}_\alpha(\theta,0)=\left(\sqrt{1-z_\alpha^2}\cos\theta,\sqrt{1-z_\alpha^2}\sin\theta,z_\alpha\right),\quad \alpha=1,\ldots,M, \tag{2.5}$$

where

$$z_\alpha=1-\frac{2\alpha}{M+1}. \tag{2.6}$$

The value of the uniform vorticity in each of the zonal regions is approximated by piecewise constant, and the jump across the contour curve $\boldsymbol{X}_\alpha$, say $\tilde{\omega}_\alpha$, is given by

$$\tilde{\omega}_\alpha=\frac{1}{2}(z_{\alpha-1}-z_{\alpha+1}), \tag{2.7}$$

in which $z_0=1$ and $z_{M+1}=-1$. The velocity field induced by the $M+1$ zonal vorticity strips is represented by the boundary integral along the M contours (see Dritschel 1989; Dritschel & Polvani 1992; Polvani & Dritschel 1993 for further relevant discussions),

$$\boldsymbol{u}_s(\boldsymbol{x})=-\sum_{\alpha=1}^{M}\omega_\alpha\int_0^{2\pi}\log|\boldsymbol{x}-\boldsymbol{X}_\alpha|^2\frac{\partial\boldsymbol{X}_\alpha}{\partial\theta}\,\mathrm{d}\theta. \tag{2.8}$$

The numerical computation becomes unstable when the vortex points approach very close to the contour curves. Thus, the interaction between the vortex points and the vorticity strips is evaluated by a velocity field regularized by the vortex blob method. Introducing a small $\delta>0$, the regularized velocity fields are given by

$$\boldsymbol{u}_{\mathrm{v}}^{(\delta)}(\boldsymbol{x})=\frac{\Gamma}{4\pi}\sum_{\alpha=1}^{N}\frac{\boldsymbol{x}_\alpha\times\boldsymbol{x}}{1+\delta^2-\boldsymbol{x}\cdot\boldsymbol{x}_\alpha}, \tag{2.9}$$

$$\boldsymbol{u}_{\mathrm{s}}^{(\delta)}(\boldsymbol{x})=-\sum_{\alpha=1}^{M}\omega_\alpha\int_0^{2\pi}\log(|\boldsymbol{x}-\boldsymbol{X}_\alpha|^2+\delta^2)\frac{\partial\boldsymbol{X}_\alpha}{\partial\theta}\,\mathrm{d}\theta. \tag{2.10}$$

The regularization parameter δ was successfully introduced to compute the long-time evolution of a vortex sheet (Kransy 1986) and is described thoroughly in the book of Cottet & Koumoutsakos (2000). The regularization stabilizes the numerical computation and makes it possible to track the evolution of the vortex points and contours. Let us briefly comment on the accuracy of the computational results. As the interaction between the vortex ring and the contours evolves, the contours roll up and form filamentary structures. In that case, the contour surgery technique (Dritschel 1989) and a continual redistribution of discretizing points are required to maintain high accuracy. Since we are primarily interested in the interaction mechanisms which work initially to destabilize the ring, we are able to get away without using the contour surgery technique. We also take sufficiently many nodal points in our initial

discretization of the contours, so redistribution of the points is not necessary. For longer simulations, both of these procedures would be needed.

Accordingly, the equations we consider are

$$\frac{\partial \boldsymbol{x}_j}{\partial t} = \boldsymbol{u}'_{\rm v}(\boldsymbol{x}_j) + \boldsymbol{u}_{\rm s}^{(\delta)}(\boldsymbol{x}_j), \quad j = 1, \ldots, N, \tag{2.11}$$

$$\frac{\partial \boldsymbol{X}_k}{\partial t} = \boldsymbol{u}_{\rm s}(\boldsymbol{X}_k) + \boldsymbol{u}_{\rm v}^{(\delta)}(\boldsymbol{X}_k), \quad k = 1, \ldots, M, \tag{2.12}$$

where $\boldsymbol{u}'_{\rm v}$ equals to the summation terms in equation (1.1). The boundary integral along each of the contours is approximated by the trapezoidal rule with 4096 points. The temporal integration of equations (2.11) and (2.12) are carried out with the fourth-order Runge–Kutta method, for which the time-step size is $\Delta t = 0.01$. The regularization parameter is fixed, $\delta = 0.1$. We have done numerical computations for various values of δ and confirmed that the qualitative numerical results are relatively insensitive to changes in δ.

3. Rings

(a) *Two-way coupled ring dynamics: co-rotation*

Consider the ring configuration shown in figure 1. The basic parameters defining the ring are its angle γ with respect to the z-axis, its opening angle θ_0, the number of point vortices distributed along the spherical cap, N, and the number of constant vorticity regions, M, used to represent the background field (see DiBattista & Polvani (1998) for some discussion on the merits and accuracy of choosing different values for M). While all of these parameters play a role in the details of the dynamical evolution of the system, our goal is to extract the main features of the effect of the misalignment $\gamma \neq 0$ during the interaction process. In Part I, figs 11–14 show the evolution of a ring in the one-way coupled model for the case $N = 4$, with orientation angles $\gamma = \pi/4$, $\pi/2$ and $3\pi/4$ and frequency ratios $\omega : \Omega = 1 : 1$; $2 : 1$ and $3 : 1$. The trajectories of the vortices in this model move on closed periodic orbits in all cases. Note that for the case $\gamma = \pi/4$, the ring co-rotates with the solid-body field, while for the case $\gamma = 3\pi/4$, it counter-rotates. The case $\gamma = \pi/2$ is a special symmetric orientation which we will describe later. The length of the centre-of-vorticity vector associated with the ring is constant, as is the Hamiltonian energy.

As a first step in understanding the two-way coupled model, we highlight a well-known fact (also seen nicely by DiBattista & Polvani 1998) that in the absence of point vortices, the contours support the propagation (see fig. 4 in DiBattista & Polvani 1998) of Rossby waves which move *retrograde* with respect to the solid-body rotation. The general processes by which Rossby waves propagate and lose stability are by now quite well documented (Hoskins 1973; Pedlosky 1987), while the mechanisms by which their coupling to structures embedded in the flow serve to break up these structures is far less understood.

Consider the sequence of simulations shown in figure 2 for the case $N = 4$, $M = 10$, $\gamma = \pi/4$ and $\theta_0 = \pi/4$ and a frequency ratio $4 : 1$. In this sequence, the ring is initially co-rotating with the background field. As seen in the figures, as the rings cut through the contours, they wrap around each of the point

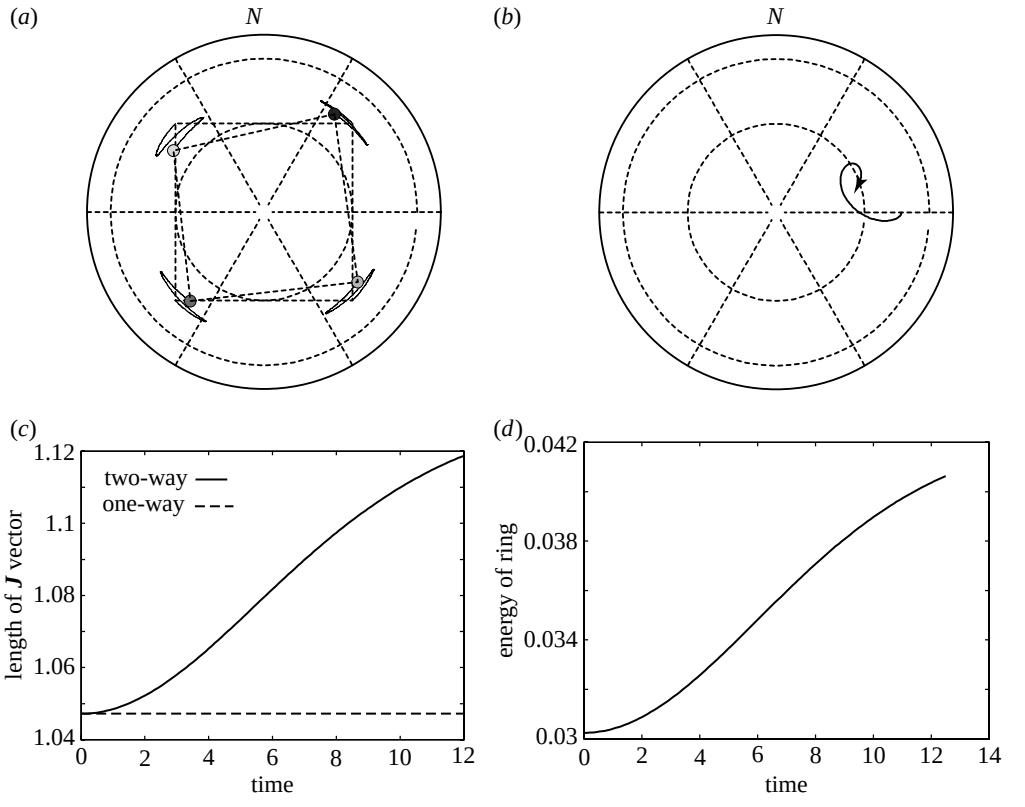

Figure 3. (*a*) Evolution of point vortices in a frame of reference rotating with the background frequency of the one-way coupled model with a frequency ratio 4 : 1. Note that the ring briefly reverses direction, but as the strength of the vortices increases, it regains its original rotational direction and remains relatively intact. (*b*) Evolution of the tip of the centre-of-vorticity vector $\boldsymbol{J}$ associated with the ring. Note that it rotates up towards the North Pole. (*c*) Evolution of the length of the centre-of-vorticity vector $\|\boldsymbol{J}\|$ which is constant in the one-way coupled model but not when the ring is coupled to the background flow. In this case, as the vortices increase their strength by wrapping themselves in the contours, the length of $\boldsymbol{J}$ increases. (*d*) The Hamiltonian is no longer conserved when the ring is coupled to the background. In this case, since the ring is co-rotating with the background, it is gaining energy from it.

vortices, thus effectively increasing their strength and triggering an instability that sets up wave propagation along the deforming contours. The effect of these waves on the ring configuration is depicted clearly in figure 3. The ring begins to rotate around its $\boldsymbol{J}$ vector, as shown in figure 3*a*, which depicts the vortex paths moving in a reference frame with the solid-body frequency Ω and shown so that the centre-of-vorticity vector is initially centred. The effect of the retrograde motion of the Rossby waves causes the rotational direction to briefly reverse with respect to this rotating frame. As the vortices increase their strength by tightly wrapping the contours around their centres, the length of the $\boldsymbol{J}$ vector associated with the ring increases and eventually the ring becomes strong enough to overcome the temporary reversal of direction caused by the incoming waves. It then assumes its original rotational direction as evidenced by the *S*-shaped vortex paths depicted in figure 3*a*. The tip of the

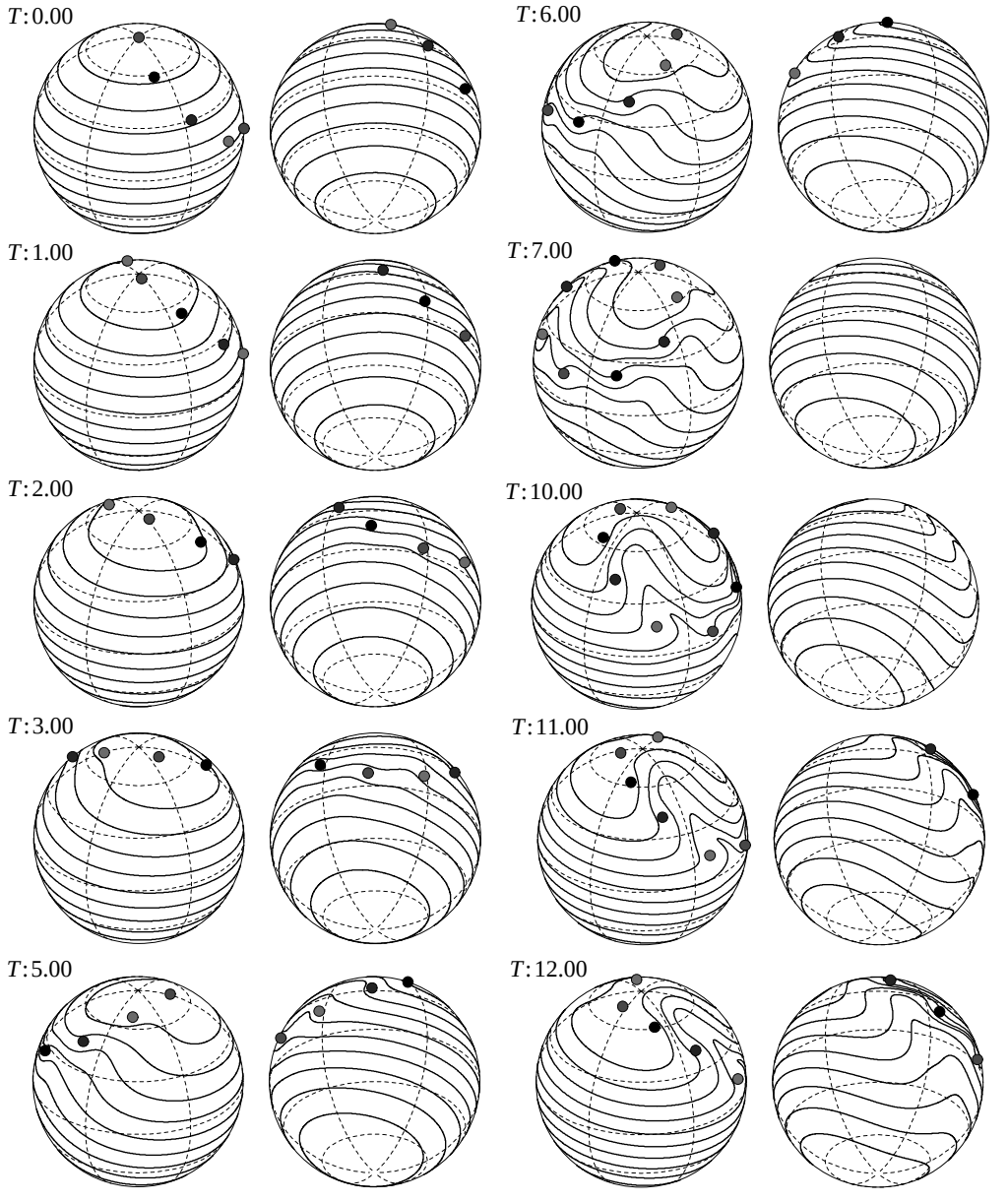

Figure 4. Evolution of ring configuration and contours with $N=8$ and $M=10$ and frequency ratio 4 : 1. Orientation $\gamma=\pi/4$ and $\theta_0=\pi/4$. $T=0.00$–12.00 in dimensionless units.

$\boldsymbol{J}$ vector, as shown in figure 3*b*, no longer cuts a clean latitudinal cap as it did in the one-way coupled model, but spirals up in a clockwise fashion towards the North Pole. Its length increases (see figure 3*c*) and the Hamiltonian energy associated with the ring (shown in figure 3*d*) gains energy from the background. This general sequence of events is quite robust to changes in the number of point vortices making up the ring, as shown in the sequence of figures 4 and 5 for $N=8$.

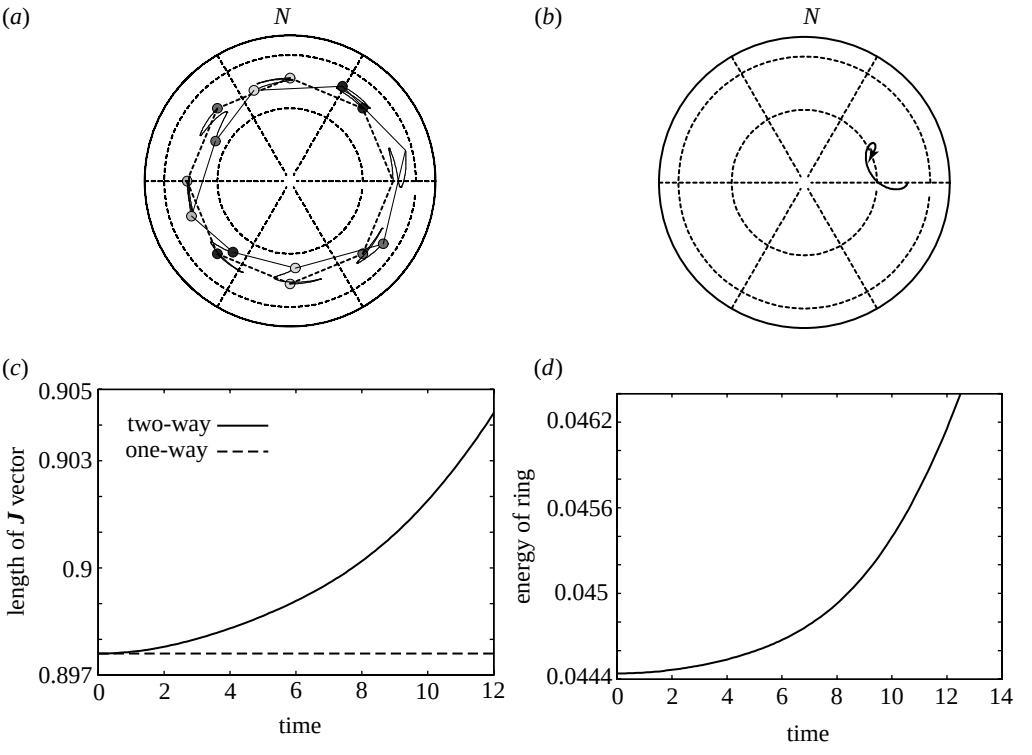

Figure 5. Same parameters as figure 3, but with $N=8$. The conclusions are robust with respect to changes in N.

(*b*) *Two-way coupled ring dynamics: counter-rotation*

A case where the ring initially counter-rotates with respect to its background is shown in figure 6 and should be contrasted with the previous sequence of figures. The parameters for this case are the same as those in figure 2, but the frequency ratio is now $-4:1$. As the contours wrap around the point vortices, their effective strength *decreases* (in absolute magnitude), causing the ring to diminish in strength relative to the background. Owing to this, it never regains its original rotational direction, as shown in figure 7*a* which should be contrasted with the corresponding figure 3*a*. In addition, the ring loses its coherence more quickly than the co-rotating case, the tip of the $\boldsymbol{J}$ vector spins towards the North Pole and decreases its effective length while losing energy to the background.

As a general observation, in all cases, the ring structure is broken (i.e. the ring is unstable) due to its interaction with the background (in contrast with the one-way coupled model), but in the case where the ring initially co-rotates with the background field, the instability neither develop as quickly, nor is it as violent as is the case when the ring counter-rotates with respect to the background.

(*c*) *$\gamma=\pi/2$: breaking symmetry*

The special case $\gamma=\pi/2$ is worth considering separately, as there is symmetry with respect to co- and counter-rotation since $\boldsymbol{J}$ is perpendicular to the axis of

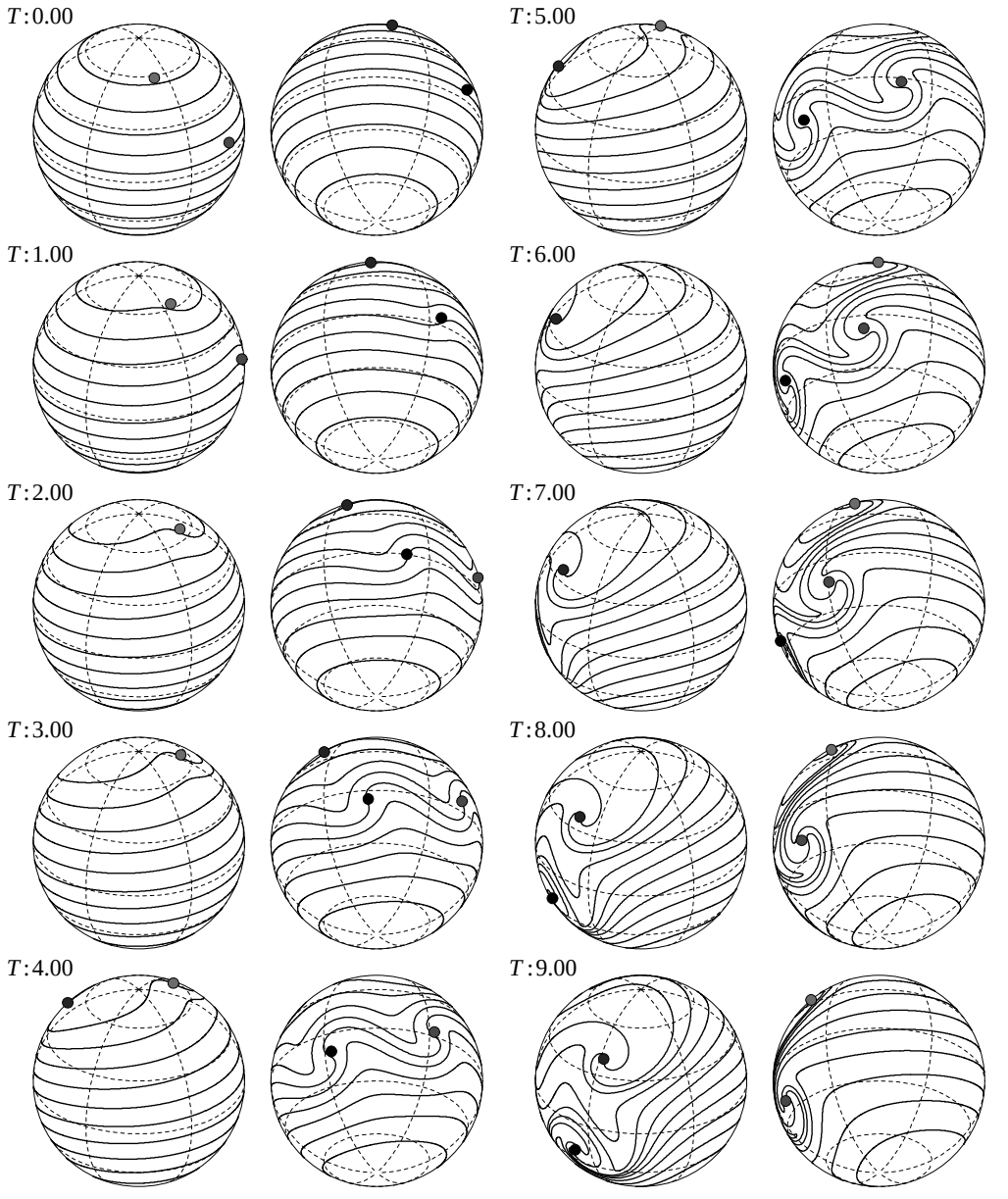

Figure 6. Evolution of ring configuration and contours with $N=4$ and $M=10$ and frequency ratio $-4:1$. Orientation $\gamma=\pi/4$ and $\theta_0=\pi/4$. $T=0.00$–9.00 in dimensionless units. In contrast to the co-rotating case, the wrapping of the contours around the point vortices causes their strength to *decrease* (in absolute magnitude) relative to the background.

rotation. As a result, we need to consider only the evolution associated with $\Gamma>0$. This case in the one-way coupled model, where the $\boldsymbol{J}$ vector remains perpendicular to the axis of rotation, is shown in fig. 13 of Part I (Newton & Shokraneh 2006*a*). For the two-way coupled case, the evolution sequence is shown in figure 8. For this orientation, the ring initially cuts the contours perpendicularly and there is no

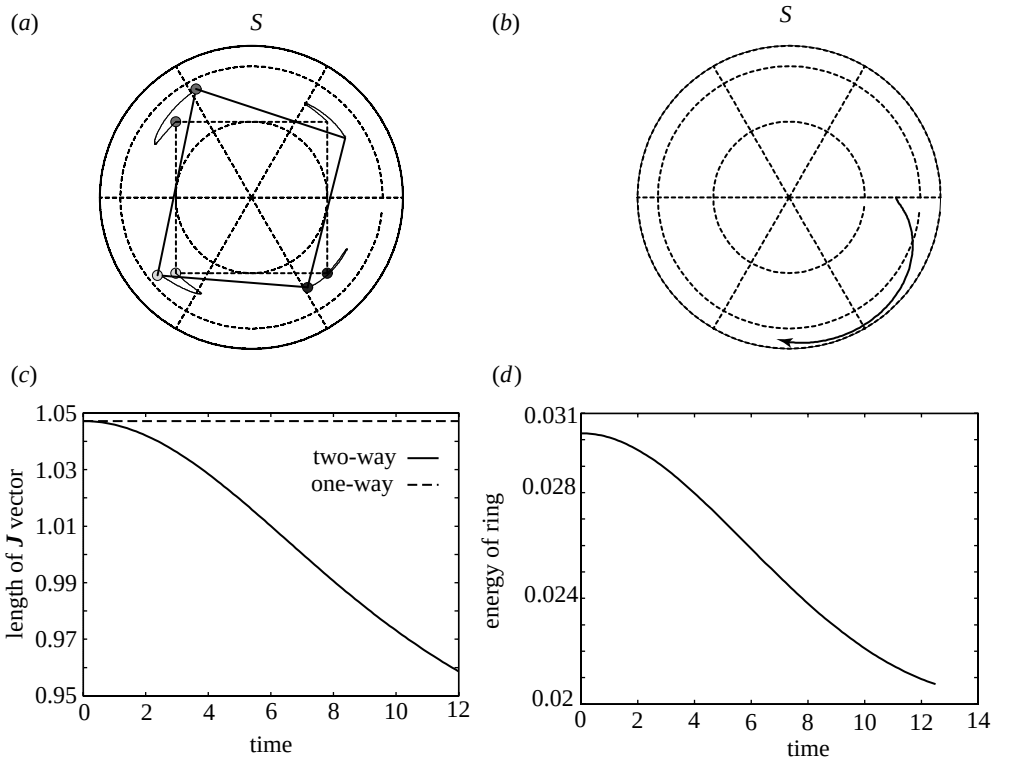

Figure 7. (*a*) Evolution of point vortices in a frame of reference rotating with the background frequency of the one-way coupled model with a frequency ratio $-4:1$. In contrast to figure 3, the original rotational direction of the ring is never regained and the ring loses its coherence much more quickly. (*b*) Evolution of the tip of the centre-of-vorticity vector $\boldsymbol{J}$ associated with the ring. Note that it still rotates towards the North Pole. (*c*) Evolution of the length of the centre-of-vorticity vector $\|\boldsymbol{J}\|$ which decreases as the contours wrap around the vortex centres. (*d*) The Hamiltonian is no longer conserved when the ring is coupled to the background. In this case, since the ring is counter-rotating with the background, it is losing energy to it.

distinction between co- and counter-rotation. In the one-way coupled model, $\boldsymbol{J}$ would remain perpendicular to the axis of rotation throughout the entire evolution, as there is no mechanism by which this symmetry is broken. In this case, however, the coupling to the background provides such a symmetry-breaking mechanism. As the vortices within the ring wrap the contours around themselves, the perfect ring structure and its orientation are destroyed immediately. The shape of the ring, the evolution of the tip of $\boldsymbol{J}$, its length and the evolution of H for this case are all shown in figure 9. Note that the characteristic S shape associated with the previously discussed co-rotating states is shown in figure 9*a*. As the contours wrap around the vortices, their strength relative to the background is able to overcome the initial reversal of direction caused by the incoming Rossby waves. Figure 9*b* shows the tip of $\boldsymbol{J}$ spiralling up towards the North Pole as before, but the evolution of its length, as shown in figure 9*c*, and the Hamiltonian energy, as shown in figure 9*d*, are more complex than any of the earlier cases. Initially, the length of both $\boldsymbol{J}$ and H increase (thereby gaining energy from the background), but then reverse direction and decreases, achieving a local maximum at roughly the same time.

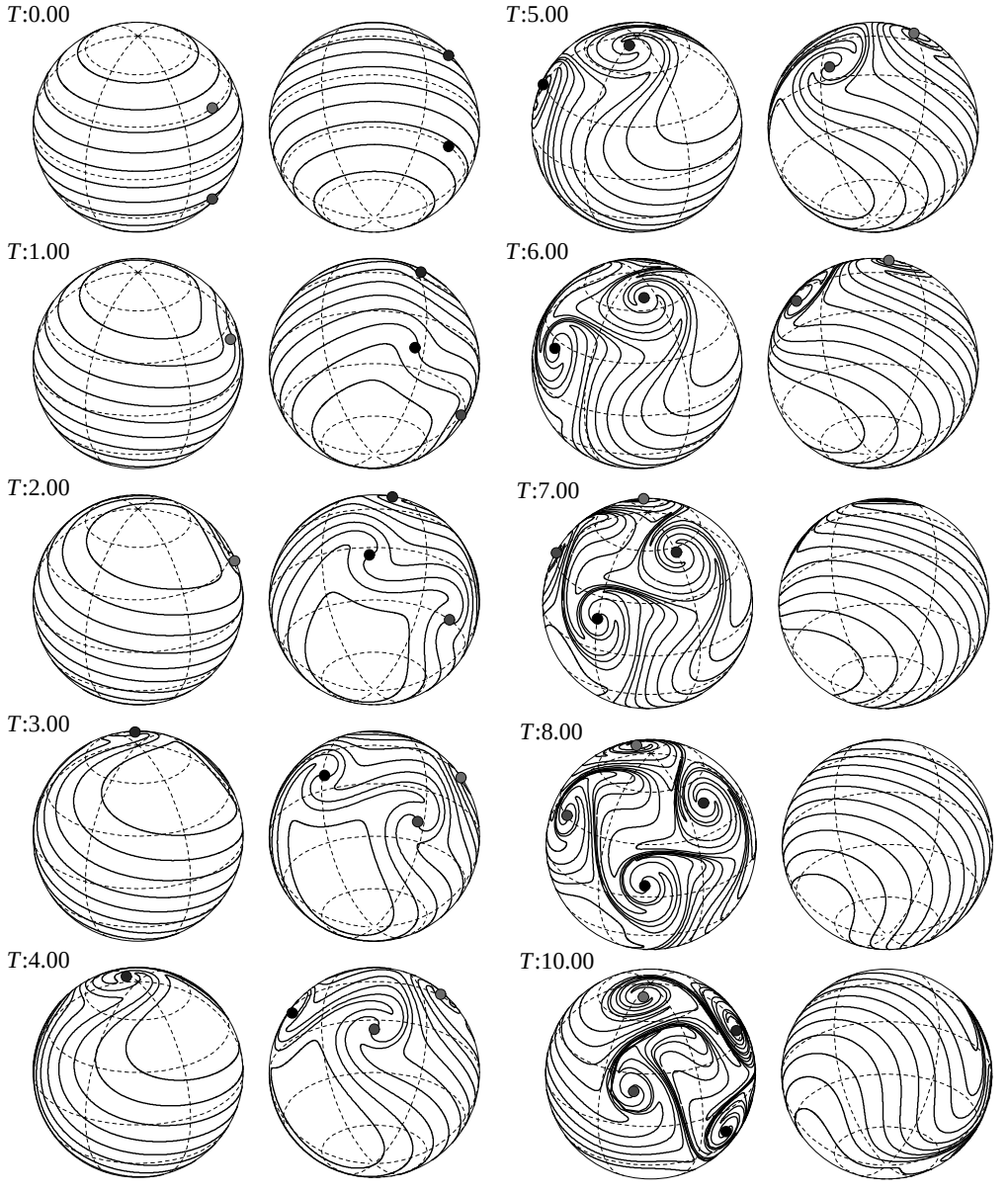

Figure 8. Evolution of ring configuration and contours with $N=4$ and $M=10$ and frequency ratio $2:1$. Orientation $\gamma=\pi/2$ and $\theta_0=\pi/4$. $T=0.00$–10.00 in dimensionless units. For this orientation, if the sign of Γ is reversed, the evolution of the system will be identical but in the opposite hemisphere. Note that the wrapping of the contours around the point vortices effectively increases their strength. The ring stays relatively intact throughout the evolution.

4. Discussion

We highlight the key sequence of events that take place due to the combined effects of the misalignment of the $\boldsymbol{J}$ vector with the axis of rotation and the coupling to the background field:

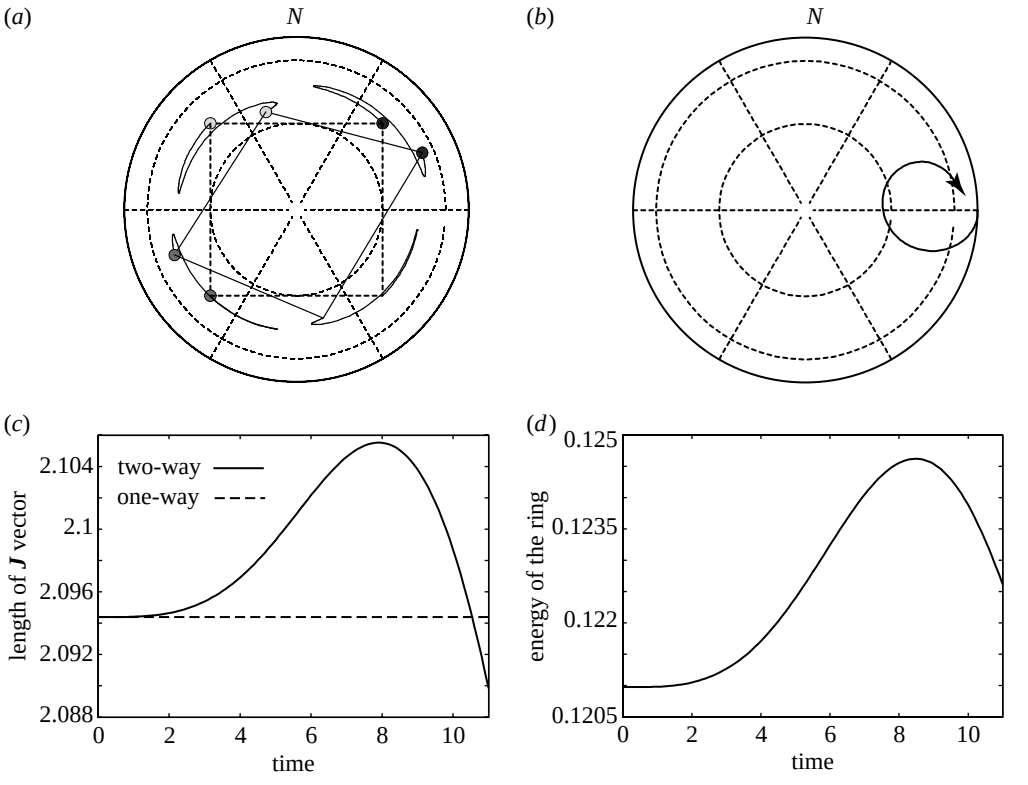

Figure 9. (*a*) Evolution of point vortices in a frame of reference rotating with the background frequency of the one-way coupled model with a frequency ratio 2 : 1 and $\gamma = \pi/2$. For this symmetric case, the ring briefly reverses direction, but as the strength of the vortices increases, it regains its original rotational direction as in the previously discussed co-rotating cases. (*b*) Evolution of the tip of the centre-of-vorticity vector $\boldsymbol{J}$ associated with the ring. (*c*) Evolution of the length of the centre-of-vorticity vector $\|\boldsymbol{J}\|$. As the vortices increase their strength by wrapping themselves in the contours, the length of $\boldsymbol{J}$ evolves in a more complex manner like either the co- or counter-rotating cases discussed previously. Initially, its length increases but reverses direction. (*d*) Evolution of the Hamiltonian energy of the ring which achieves a local maximum at roughly the same time as $\|\boldsymbol{J}\|$.

— the ring triggers an instability in the background field setting up Rossby waves which travel along the contours moving retrograde to the solid-body rotation direction;
— these waves cause the ring to alter its rotational direction;
— the contours wrap around the point vortices, increasing their effective strength in the case where the ring co-rotates with the background, decreasing it (in absolute magnitude) in the case when it counter-rotates;
— the increase in strength in the co-rotating case allows the ring to overcome the effects of the Rossby waves and reverse direction again, regaining its original rotational direction;
— in the counter-rotating case, since the ring strength is effectively decreasing, the ring never regains its original rotational direction;
— energy is continually exchanged between the ring and the background field (i.e. H and $\|\boldsymbol{J}\|$ are no longer conserved) via this process of contour wrapping and the stability and integrity of the ring is compromised;

— in the special symmetric configuration when $\boldsymbol{J}$ is initially perpendicular to the axis of rotation of the background field, the coupling provides a symmetry-breaking mechanism not present in the one-way coupled model. The evolution of $\|\boldsymbol{J}\|$ and H are non-monotonic, both reaching a local maximum at roughly the same time.

A key feature of the one-way coupled model discussed in Part I was that the integrability of the non-rotating problem ($\Omega=0$) and the rotating problem ($\Omega\neq 0$) were identical. With the two-way coupled model, on the short time-scale, the coupling to the background offers a mechanism by which the ring is destabilized and loses its coherence. On a longer time-scale, since all of the main conserved quantities ($\boldsymbol{J}$ and H) are broken, it offers a natural mechanism by which integrability is destroyed and we expect that the long-time evolution of the vortices will be chaotic. Of course, tracking them accurately for long enough time-scales to compute quantities such as Lyapunov exponents is far more challenging than in the one-way coupled case. This is primarily owing to the aggressive growth and wrapping of the many contours that must be tracked. In a simpler setting, the growth of these types of interfaces and their connection with the mixing and transport of passive particles has been studied by Newton & Ross (2006) for a perturbed point-vortex ring on the sphere without rotation. In the two-way coupled problem, it is the coupling to the background that causes the ring perturbation. This, in turn, generates the Rossby waves which we identify as the main physical mechanism responsible for breakdown of the integrability and loss of coherence of the ring.

References

Bogomolov, V. A. 1977 Dynamics of vorticity at a sphere. *Fluid Dyn.* **6**, 863–870. (doi:10.1007/BF01090320)

Bogomolov, V. A. 1979 Two dimensional fluid dynamics on a sphere. *Izv. Atmos. Ocean. Phys.* **15**, 18–22.

Bogomolov, V. A. 1985 On the motion of a vortex on a rotating sphere. *Izv. Atmos. Ocean. Phys.* **21**, 298–302.

Cabral, H. E., Meyer, K. R. & Schmidt, D. S. 2003 Stability and bifurcations for the $N+1$ vortex problem on the sphere. *Regul. Chaotic Dyn.* **8**, 259–282. (doi:10.1070/RD2003v008n03ABEH000243)

Cottet, G.-H. & Koumoutsakos, P. D. 2000 *Vortex methods: theory and practice*. Cambridge, UK: Cambridge Press.

DiBattista, M. T. & Polvani, L. M. 1998 Barotropic vortex pairs on a rotating sphere. *J. Fluid Mech.* **358**, 107–133. (doi:10.1017/S0022112097008100)

Dritschel, D. G. 1989 Contour dynamics and contour surgery: numerical algorithms for extended high resolution numerical modeling of vortex dynamics in two-dimensional, inviscid, incompressible flows. *Comp. Phys. Rep.* **10**, 77–146. (doi:10.1016/0167-7977(89)90004-X)

Dritschel, D. G. & Polvani, L. M. 1992 The roll-up of vorticity strips on the surface of a sphere. *J. Fluid Mech.* **234**, 47–69. (doi:10.1017/S0022112092000697)

Hoskins, B. J. 1973 Stability of the Rossby-Haurwitz wave. *Q J. R. Meteor. Soc.* **99**, 723. (doi:10.1256/smsqj.42212)

Jamaloodeen, M. I. & Newton, P. K. 2006 The N-vortex problem on a rotating sphere: II. Heterogeneous Platonic solid equilibria. *Proc. R. Soc. A* **462**, 3277–3299. (doi:10.1098/rspa.2006.1731)

Kidambi, R. & Newton, P. K. 1998 Motion of three point vortices on a sphere. *Physica D* **116**, 143–175. (doi:10.1016/S0167-2789(97)00236-4)

Kidambi, R. & Newton, P. K. 2000 Streamline topologies for integrable vortex motion on a sphere. *Physica D* **140**, 95–125. (doi:10.1016/S0167-2789(99)00233-X)

Kransy, R. 1986 Desingularization of periodic vortex sheet roll-up. *J. Comp. Phys.* **65**, 292–313. (doi:10.1016/0021-9991(86)90210-X)

Majda, A. 2003 *Introduction to PDEs and waves for the atmosphere and ocean.* Courant Institute Lecture Notes, vol. 9. Providence, RI: American Mathematical Society.

Marcus, P. S. 1993 Jupiter's great red spot and other vortices. *Annu. Rev. Astron. Astrophys.* **31**, 523–573. (doi:10.1146/annurev.aa.31.090193.002515)

McDonald, N. R. 1999 The motion of geophysical vortices. *Phil. Trans. R. Soc. A* **357**, 3427–3444. (doi:10.1098/rsta.1999.0501)

Newton P. K. 2001 The *N*-vortex problem: analytical techniques. Lecture Notes in Applied Mathematical Sciences, vol. 145, New York, NY: Springer.

Newton, P. K. & Ross, S. D. 2006 The restricted four vortex problem. *Physica D* **223**, 36–53. (doi:10.1016/j.physd.2006.08.012)

Newton, P. K. & Shokraneh, H. 2006*a* The *N*-vortex problem on a rotating sphere: I. Multi-frequency configurations. *Proc. R. Soc. A* **462**, 149–169. (doi:10.1098/rspa.2005.1566)

Newton P. K. & Shokraneh H. 2006*b* The *N*-vortex problem on a rotating sphere: IV. Dipoles as interacting billiards. Preprint, USC.

Pedlosky, J. 1987 *Geophysical fluid dynamics*, 2nd edn. New York, NY: Springer.

Polvani, L. M. & Dritschel, D. G. 1993 Wave and vortex dynamics on the surface of a sphere. *J. Fluid Mech.* **255**, 35–64. (doi:10.1017/S0022112093002381)